

OPEN

# Enhanced electrochemical performance of lithia/ $\text{Li}_2\text{RuO}_3$ cathode by adding tris(trimethylsilyl)borate as electrolyte additive

Byeong Gwan Lee &amp; Yong Joon Park

In this study, we used tris(trimethylsilyl)borate (TMSB) as an electrolyte additive and analysed its effect on the electrochemical performance of lithia-based (Lithia/ $\text{Li}_2\text{RuO}_3$ ) cathodes. Our investigation revealed that the addition of TMSB modified the interfacial reactions between a lithia-based cathode and an electrolyte composed of the carbonate solvents and the  $\text{LiPF}_6$  salt. The decomposition of the  $\text{LiPF}_6$  salt and the formation of  $\text{Li}_2\text{CO}_3$  and  $-\text{CO}_2$  was successfully reduced through the use of TMSB as an electrolyte additive. It is inferred that the protective layer derived from the TMSB suppressed the undesirable side reaction associated with the electrolyte and superoxides ( $\text{O}^-$  or  $\text{O}^{0.5-}$ ) formed in the cathode structure during the charging process. This led to the reduction of superoxide loss through side reactions, which contributed to the increased available capacity of the Lithia/ $\text{Li}_2\text{RuO}_3$  cathode with the addition of TMSB. The suppression of undesirable side reactions also decreased the thickness of the interfacial layer, reducing the impedance value of the cells and stabilising the cyclic performance of the lithia-based cathode. This confirmed that the addition of TMSB was an effective approach for the improvement of the electrochemical performance of cells containing lithia-based cathodes.

One of the most important issues relating to lithium-ion batteries (LIBs) is the development of new cathodes with higher energy densities than commercially used  $\text{LiCoO}_2$ ,  $\text{Li}(\text{Ni}, \text{Co}, \text{Mn})\text{O}_2$  (NCM), and  $\text{Li}(\text{Ni}, \text{Co}, \text{Al})\text{O}_2$  (NCA)<sup>1–7</sup>. Fundamentally, the capacity of most cathodes can be attributed to the cationic redox of transition metals such as Co, Ni, and Mn in the structure. Therefore, it is necessary to increase the amount of transition metals (per weight or volume) in the cathode structure to improve its energy density, which is not an easy task considering the crystal structure of transition metal oxides. However, if the redox reaction of the anions (such as oxygen ions) can contribute to the capacity of the cathode, this problem can be overcome. The anions are much lighter than general transition ions, therefore the cathodes can provide much higher capacity (per weight) and energy density compared to cases relying on only cationic redox reactions. Subsequently, cathodes based on anionic redox reactions have been attractive research topics of late. As promising new cathode materials,  $\text{Li-Nb-Mn-O}$ ,  $\text{Li-Mn-O}$ , and  $\text{Li-Ru-M-O}$  ( $M = \text{Sn}, \text{Nb}$ ) have been studied for years<sup>8–13</sup>. These materials have shown high capacity—up to approximately  $300 \text{ mA}\cdot\text{g}^{-1}$  based on anionic redox associated with oxygen as well as cationic redox related to transition metals. However, their sluggish kinetics and structural instability have resulted in an inferior rate capacity and cyclic performance compared to commercial cathodes<sup>8–13</sup>.

Lithia ( $\text{Li}_2\text{O}$ )-based materials are also one of the new candidates for high-capacity cathodes based on anionic redox reactions<sup>14–20</sup>. In fact, most of the new cathodes such as  $\text{Li-Nb-Mn-O}$ ,  $\text{Li-Mn-O}$ , and  $\text{Li-Ru-M-O}$  ( $M = \text{Sn}, \text{Nb}$ ) provide capacity primarily based on the cationic redox reaction, although some portion of the capacity is clearly attributed to the anionic redox reaction. By contrast, the capacity of lithia-based cathodes is mostly related to the anionic redox reaction between oxygen ions ( $\text{O}^{2-}$ ) in the structure and superoxides ( $\text{O}^x$ ,  $0.5 \leq X < 2$ ). Moreover, their cyclic performance is stable if the capacity is limited to avoid the formation of gaseous oxygen or the generation of superoxides above a threshold. However, lithia-based cathodes require suitable

Department of Advanced Materials Engineering, Kyonggi University, 154-42, Gwanggyosan-ro, Yeongtong-gu, Suwon-si 16227, Gyeonggi-do, Republic of Korea. email: yjpark2006@kyonggi.ac.kr

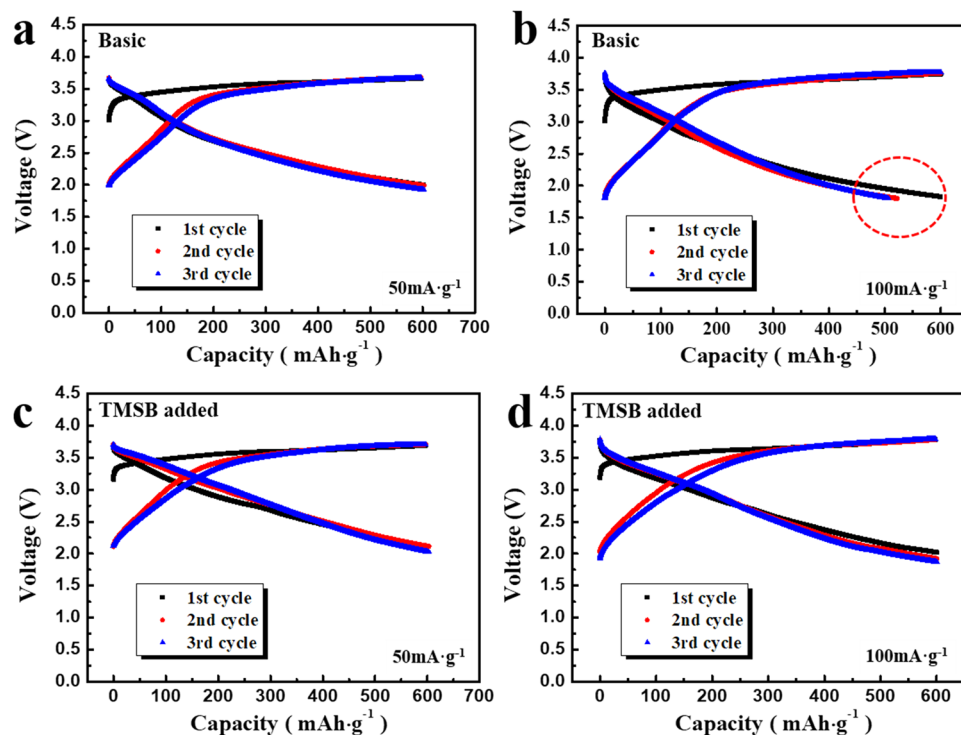


**Figure 1.** Charge–discharge profiles of the cells containing lithia/ $\text{Li}_2\text{RuO}_3$  nanocomposite with limited capacity of  $600 \text{ mAh}\cdot\text{g}^{-1}$ , measured (a) at  $50 \text{ mA}\cdot\text{g}^{-1}$  using the basic electrolyte, (b) at  $100 \text{ mA}\cdot\text{g}^{-1}$  using the basic electrolyte, (c) at  $50 \text{ mA}\cdot\text{g}^{-1}$  using TMSB added electrolyte, and (d) at  $100 \text{ mA}\cdot\text{g}^{-1}$  using TMSB added electrolyte.

catalysts (sometimes called dopants) because lithia is not in itself electrochemically active. Therefore, the research of lithia-based cathodes to date has focused on the exploration of good catalysts for lithia and the combination between the catalysts and lithia<sup>14–20</sup>. However, a fact that cannot be overlooked is that lithia-based cathodes are vulnerable to organic electrolytes, as are most cathodes. In particular, the basic reaction mechanism of lithia-based cathodes that form superoxides ( $\text{O}^{\cdot-}$ ,  $0.5 \leq X < 2$ ) in the structure during cycling may promote undesirable reactions between liquid electrolytes. Therefore, research to stabilise the interface between the cathode and the electrolyte is essential in order to obtain stable electrochemical performance from lithia-based cathodes. Nevertheless, such studies are still at a rudimentary stage.

A representative approach to improve interfacial stability between a cathode and an electrolyte is surface coating of the cathode, which is widely used for commercial LIBs<sup>21–27</sup>. However, it is difficult to apply to lithia-based cathodes because a coating process utilising heat-treatment may significantly deteriorate lithia-based cathodes due to the extremely reactive lithia. Whereas, the use of electrolyte additives may be a promising solution to the interfacial problem of lithia-based cathodes<sup>28–29</sup>. The additives dissolve in the decomposed electrolyte during cycling to form a protective layer on the surface of the cathode. Since they are not used directly on the cathode, they can be applied to highly reactive lithia-based cathodes without any trouble.

In this study, tris(trimethylsilyl)borate (TMSB) was introduced as an electrolyte additive for a lithia-based cathode. TMSB reportedly forms a stable film layer on the surface of the cathode, which stabilises the cathode/electrolyte interface<sup>30–34</sup>. For a lithia-based cathode, lithia/ $\text{Li}_2\text{RuO}_3$  nanocomposites were used due to their high capacity and good cycle life<sup>20</sup>. The most anticipated effect of this study was the increase in the available capacity of the lithia/ $\text{Li}_2\text{RuO}_3$  nanocomposites. In general, the capacity of commercial cathodes was not critically affected by the electrolyte additive, but the effect of the additive significantly enhanced the rate capability, cyclic performance, and efficiency of the cells. By contrast, some lithia-based cathodes showed improved available capacity through the addition of electrolyte additives<sup>28–29</sup>, a fairly unique outcome. In this work, the electrochemical performance of lithia/ $\text{Li}_2\text{RuO}_3$  nanocomposites through the addition of TMSB was carefully characterised.

**Electrochemical performance.** For convenience, the electrolyte without TMSB was named ‘basic’ electrolyte in this work. To evaluate the influence of TMSB on the electrochemical properties, the discharge capacity, and the cyclic performance of the cells containing lithia/ $\text{Li}_2\text{RuO}_3$  nanocomposites, the cathodes were tested using the basic and TMSB added electrolytes. Figure 1 shows the charge–discharge profiles of the cells for three cycles. To compare the available capacity of the cells due to the difference in electrolytes, the measuring capacity was limited to  $600 \text{ mAh}\cdot\text{g}^{-1}$  based on the lithia weight of the cathodes. The capacity of lithia-based cathodes was limited during cycling to afford them an obtainable available capacity whilst avoiding the capacity fading attributable to cathode instability due to overcharging<sup>15–20</sup>. At a current density of  $50 \text{ mA}\cdot\text{g}^{-1}$ , the cell using the basic electrolyte showed a stable charge–discharge profile and retained its limited capacity of  $600 \text{ mAh}\cdot\text{g}^{-1}$  for three cycles (Fig. 1a). The initial charge profile was different from the subsequent charge profiles, inferring that

an irreversible reaction of the cathode had occurred during the initial cycle. When the current density increased to  $100 \text{ mA}\cdot\text{g}^{-1}$ , the cell using the basic electrolyte did not retain its limited capacity ( $600 \text{ mAh}\cdot\text{g}^{-1}$ ) during cycling. As shown in Fig. 1b, the capacity decreased during the second cycle, indicating that the available capacity of the cell using the basic electrolyte was below  $600 \text{ mAh}\cdot\text{g}^{-1}$ . By contrast, as shown in Fig. 1c, d, the cells using TMSB added electrolyte showed a stable charge–discharge profile over three cycles at  $50 \text{ mA}\cdot\text{g}^{-1}$  as well as at  $100 \text{ mA}\cdot\text{g}^{-1}$ . Although the overpotential of the cells increased at a current density of  $100 \text{ mA}\cdot\text{g}^{-1}$  compared to those at  $50 \text{ mA}\cdot\text{g}^{-1}$ , the limited capacity of the cells ( $600 \text{ mAh}\cdot\text{g}^{-1}$ ) was maintained.

Figure S1 shows the comparison of the cyclic performance of the cells using the basic and TMSB added electrolytes for 50 cycles with a limited capacity of  $600 \text{ mAh}\cdot\text{g}^{-1}$ . The cells using the basic electrolyte maintained their capacity for only 12 cycles and 1 cycle at current densities of 50 and  $100 \text{ mA}\cdot\text{g}^{-1}$ , respectively (Fig. S1a, b). However, when the TMSB was added to the electrolyte, the cells maintained their limited capacity for the full 50 cycles, indicating that the available capacity of the lithia/ $\text{Li}_2\text{RuO}_3$  nanocomposites was increased by the use of the TMSB additives (Fig. S1c, d).

Fundamentally, the capacity of a lithia-based cathode is attributed to the redox reaction of lithia ( $\text{Li}_2\text{O}$ ). The oxygen ions ( $\text{O}^{2-}$ ) in the lithia are oxidised to superoxides ( $\text{O}^-$  or  $\text{O}^{0.5-}$ ) during charging, maintaining a condensed phase in the oxide structure<sup>17–20</sup>, and the superoxides are reduced during discharging. When the lithia-based cathodes are overcharged, the oxygen ions in the cathode can be oxidised to gaseous oxygen, resulting in the evaporation of oxygen and rapid capacity fading of the cathodes. Even if the oxygen ions are not oxidised to oxygen gas, the increase in superoxides ( $\text{O}^-$  or  $\text{O}^{0.5-}$ ) in the cathodes structure are also an unstable factor since reactive superoxides react easily with the electrolyte which leads to capacity fading of the cathodes. Therefore, the capacity of a lithia-based cathode should be limited during cycling to avoid side reactions derived from superoxides as well as oxygen generation. The catalysts in a lithia-based cathode (such as Ru or Ru oxides in the lithia/ $\text{Li}_2\text{RuO}_3$  nanocomposites) act as superoxide stabilisers. However, if the quantity of superoxide in the structure increases due to overcharging, the catalyst may reach its limit, and undesirable side reactions by superoxides can no longer be prevented.

As shown in Fig S1a, b, the unstable capacity of the cells using the basic electrolyte means that oxygen ions in the lithia/ $\text{Li}_2\text{RuO}_3$  nanocomposite structures are overly oxidised to superoxides ( $\text{O}^-$  or  $\text{O}^{0.5-}$ ). Thus, when the cathode is charged to  $600 \text{ mAh}\cdot\text{g}^{-1}$ , the quantity of them is beyond the limit at which the superoxides can retain their phase in the structure without undesirable reactions. By contrast, the stable cyclic performance of the cells using TMSB added electrolyte indicates that the superoxides in the cathode charged to  $600 \text{ mAh}\cdot\text{g}^{-1}$  are stabilised by the effect derived from the TMSB (Fig S1c, d). It should be considered that the quantity of superoxides in the cathodes was not changed by the use of TMSB, as the redox reaction of the oxygen ions occurs to provide the same  $600 \text{ mAh}\cdot\text{g}^{-1}$  capacity. Therefore, it is reasonable to suggest that the superoxides formed by the charging process were stabilised in the structure due to the role of TMSB.

Figure 2a, b compare the first and second charge–discharge profiles of the cells using the basic and TMSB added electrolytes. Regardless of the type of electrolyte used, the shape of the profiles was similar. However, the overpotential of the cells was reduced by the addition of TMSB, suggesting that the TMSB added electrolyte may reduce resistance factors during cycling. It is notable that the shape of the charge–discharge profiles after 50 cycles changed significantly due to the use of the TMSB additive. As shown in Fig. 2c, when the basic electrolyte was used, the charge–discharge profile at the 50th cycle exhibited two distinct steps, which may be associated with the degradation of lithia-based cathodes during cycling. By contrast, when the TMSB added electrolyte was used, the charge–discharge curve after 50 cycles showed a relatively smooth profile without any clear voltage step, as shown in Fig. 2d. Although the overpotential increased, it appears that the cathodes were not critically damaged during cycling.

**Characterization of interfacial reaction.** From the results of the charge–discharge profile and cyclic performance, it was confirmed that the addition of TMSB in the electrolyte enhanced the electrochemical performance of the cells containing lithia/ $\text{Li}_2\text{RuO}_3$  nanocomposites. It was expected that the TMSB dissolved in the electrolyte would decompose (oxidise) during the charging process to form a stable protective layer on the surface of the cathodes. To observe the morphological change caused by the addition of TMSB, lithia-based cathodes were analysed using scanning electron microscopy (SEM) and transmission electron microscopy (TEM). Figure S2 shows the SEM images of the cathodes composed of lithia/ $\text{Li}_2\text{RuO}_3$  nanocomposites and carbon nanotubes (CNTs) before and after cycling. As shown in Fig. S2a, the particles of the lithia/ $\text{Li}_2\text{RuO}_3$  nanocomposites and CNTs seemed to have agglomerated each other before the electrochemical test. Interestingly, the agglomeration of the particles was considerably suppressed after the first cycle, as shown in Fig. S2b, c. This may have been associated with the volume contraction/expansion of the lithia ( $\text{Li}_2\text{O}$ ) due to lithiation/delithiation during cycling. After 50 cycles, the cathodes appeared to be composed of small-sized nanoparticles, as shown in Fig. S2d, e.

To analysis the surface of the cathode in detail, the TEM images of the pristine (before the electrochemical test) and cycled cathode-particles using the basic and TMSB added electrolytes were observed. As shown in Fig. 3a, the surface of the cathode-particle before the electrochemical test was clear without a heterogeneous surface layer. However, the surface was dramatically changed after 50 cycles with the limited capacity of  $600 \text{ mAh}\cdot\text{g}^{-1}$  (current density =  $100 \text{ mA}\cdot\text{g}^{-1}$ ). As shown in Fig. 3b, the cathode-particle cycled with the basic electrolyte was covered by a thick interfacial layer (20–50 nm). This kind of interfacial layer can be formed from the decomposition of a solvent such as ethylene carbonate (EC) and a salt such as  $\text{LiPF}_6$  in the electrolyte due to their reaction with the cathode surface. In fact, it has been known that the decomposition of an electrolyte occurs mainly at high voltages (over the range 4.2–4.3 V)<sup>30–34</sup>. Given the fact that most of the charging process of the cells containing lithia/ $\text{Li}_2\text{RuO}_3$  nanocomposites takes place below 4.0 V, it is doubtful that this thick interfacial

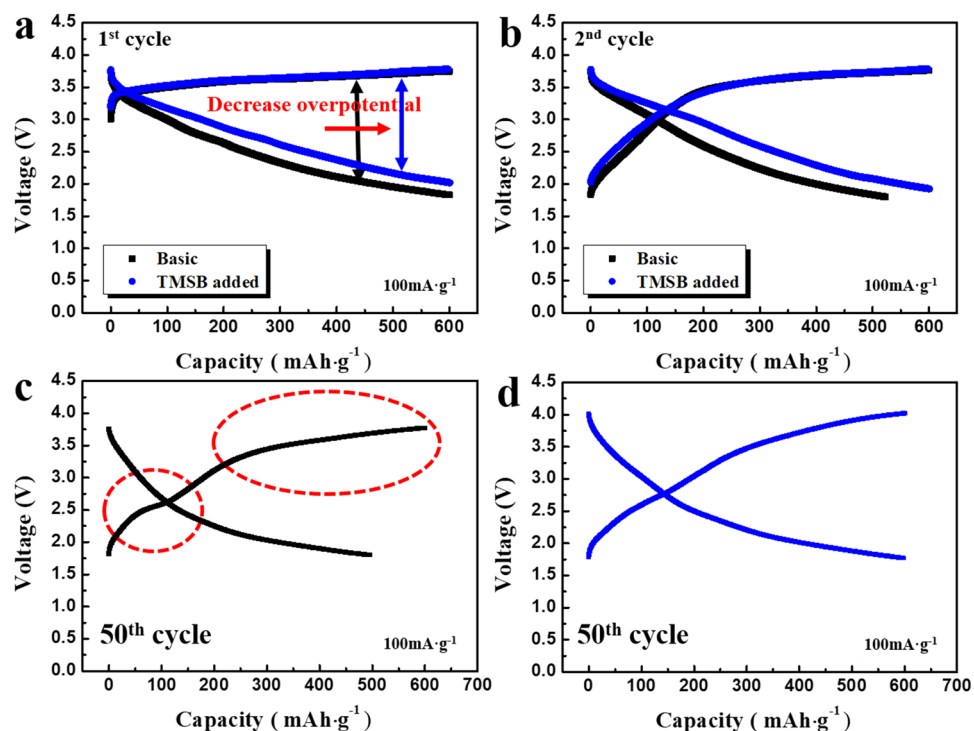


**Figure 2.** Voltage profiles of cells containing lithia/ $\text{Li}_2\text{RuO}_3$  nanocomposite at a current density of  $100 \text{ mA}\cdot\text{g}^{-1}$  with a limited capacity of  $600 \text{ mAh}\cdot\text{g}^{-1}$  (a) the first cycle using the basic and TMSB added electrolytes, (b) the second cycle using the basic and TMSB added electrolytes, (c) the 50th cycle using the basic electrolyte, and (d) the 50th cycle using TMSB added electrolyte.

layer can be attributed to the decomposition of the electrolyte. However, the lithia-based cathode generates many superoxides with high reactivity during the charging process. The superoxides ( $\text{O}^-$  or  $\text{O}^{0.5-}$ ) can activate the decomposition of the electrolyte while consuming themselves by reaction with the solvent or salt. As shown in Figs. 1 and S1, the cells using the basic electrolyte could not retain their limited capacity of  $600 \text{ mAh}\cdot\text{g}^{-1}$  during cycling. As mentioned, this shows that cells charged to  $600 \text{ mAh}\cdot\text{g}^{-1}$  were in an overcharged state and the quantity of superoxides in the cathodes exceeded the critical point at which they could stably exist in the structure of the cathode without side reactions. Therefore, the thick interfacial layer in the cycled cathode (Fig. 3b) was due primarily to the undesirable reactions between the electrolyte and superoxides in the cathode structure.

Notably, the interfacial layer was dramatically reduced by the addition of TMSB in the electrolyte. As shown in Fig. 3c, the cathode cycled 50 times using TMSB added electrolyte exhibited a relatively thin interfacial layer. We inferred that the TMSB in the electrolyte formed a stable protection layer, which successfully prevented the progress of undesirable interfacial reactions related to superoxides. Therefore, the loss of superoxides in the structure can be prevented during cycling, even if their quantity reaches the point at which they cannot retain stability using the basic electrolyte. The addition of TMSB to the electrolyte led to an increase in available capacity of the cells containing lithia-based cathodes (lithia/ $\text{Li}_2\text{RuO}_3$  nanocomposites).

Figure 4 shows the Nyquist plots of the cells containing lithia/ $\text{Li}_2\text{RuO}_3$  nanocomposites prepared using the basic and TMSB added electrolytes. The test was performed after the 1st and 50th cycles with the limited capacity of  $600 \text{ mAh}\cdot\text{g}^{-1}$ . As shown in Fig. 4, the semicircle size of the Nyquist plots of the cells was decreased by the use of TMSB regardless of the number of cycles, indicating that the impedance value of the cells was efficiently reduced by the effect of TMSB addition. The impedance value of the cells significantly increased after 50 cycles (Fig. 4b) compared to those after the first cycle (Fig. 4a). Nevertheless, the cell using TMSB added electrolyte showed much lower impedance value compared to the cell using the basic electrolyte. This result could be connected with the above TEM images as shown in Fig. 3b,c. The thick interfacial layer of the cathode cycled using a basic electrolyte may interfere with the movement of lithium ions and electrons during cycling, which results in the increase in impedance value of the cells. In contrast, the relatively thin and homogeneous interfacial layer of the cathode cycled using a TMSB added electrolyte leads to the much smaller impedance value than that of the cathode using the basic electrolyte.

To elucidate the TMSB effect, it is necessary to characterise the reaction products formed on the cathode/electrolyte interface. The electrodes containing lithia/ $\text{Li}_2\text{RuO}_3$  nanocomposites were collected from the cells before and after cycles with a limited capacity of  $600 \text{ mAh}\cdot\text{g}^{-1}$ , and their X-ray photoelectron spectroscopy (XPS) profiles were analysed. Figure S3 shows the Si 2p and B 1s spectra of the electrodes cycled with the basic and TMSB added electrolyte. As shown in Fig. S3a, b, the spectra for the electrode cycled with the basic electrolyte did not exhibit clear peaks. By contrast, the spectra for the electrode after 1 cycle with TMSB added electrolyte showed clear peaks related to Si–O and B–O. Considering Si–O and B–O bonds derived from TMSB<sup>33–35</sup>, this

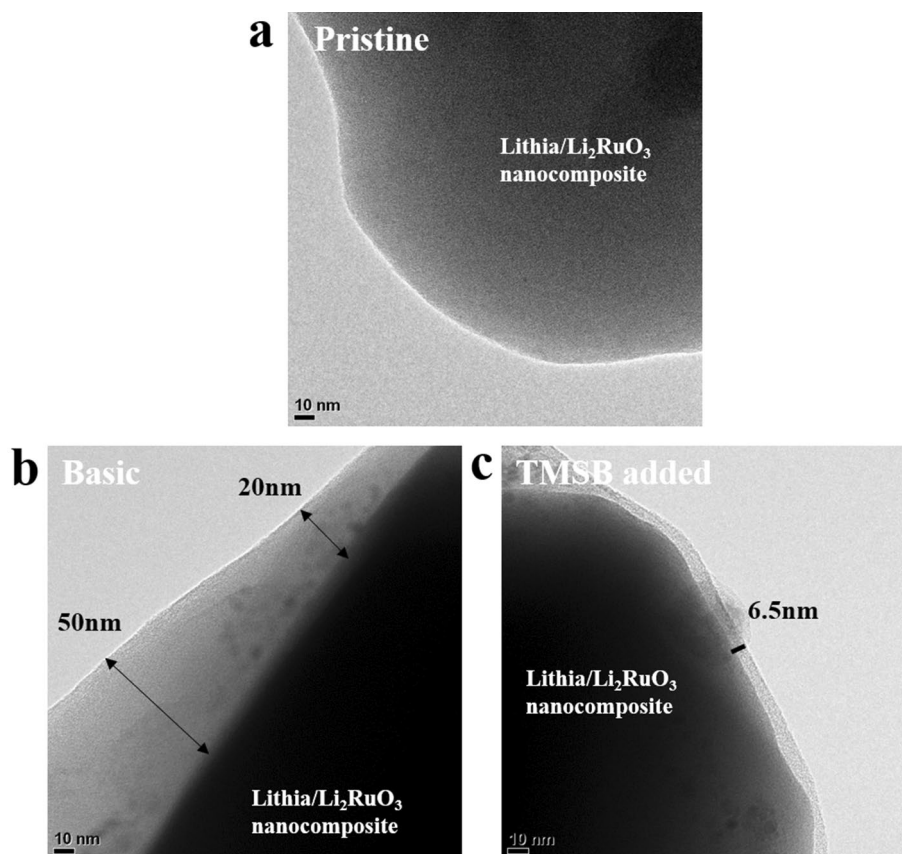


**Figure 3.** TEM images of the electrodes containing lithia/ $\text{Li}_2\text{RuO}_3$  nanocomposite (a) before the electrochemical test, (b) after 50 cycles using the basic electrolyte, and (c) after 50 cycles using TMSB added electrolyte. (The cycle test was performed using a limited capacity of  $600 \text{ mAh}\cdot\text{g}^{-1}$ ).

confirmed that TMSB was decomposed during the initial cycle, and an interfacial layer was successfully formed on the surface of the cathode. The Si–O and B–O peaks were observed in the XPS spectra of the electrode after 50 cycles, as shown in Figs. S3c and S3d. However, their intensity did not increase much, indicating that further formation of the interfacial layer derived from TMSB was limited.

Figure 5 shows the C 1s and F 1s spectra of the electrode before and after one cycle. In the C 1s spectrum of the electrode before cycling (Fig. 5a), the C–C bond ( $\sim 284.5 \text{ eV}$ ) corresponded with the conductive carbon in the electrode<sup>36–37</sup>, and C–H ( $\sim 285.5 \text{ eV}$ ) and C–F<sub>2</sub> ( $\sim 290.8 \text{ eV}$ ) bonds could be attributed to the binder (PVDF). The C–O–C ( $\sim 286.7 \text{ eV}$ ) bond was due to residual carbon and the binder<sup>38</sup>. In the F 1s spectrum of the electrode before cycling (Fig. 5b), the C–F<sub>2</sub> ( $\sim 688 \text{ eV}$ ) was associated with the PVDF binder in the electrode. A peak attributed to LiF ( $\sim 685.1 \text{ eV}$ ) was also observed, which may have been related to the reaction with lithia ( $\text{Li}_2\text{O}$ ) in the electrode. After one cycle, the generation of new peaks were observed in the C 1s spectra of the electrodes, as shown in Fig. 5c,e.  $\text{Li}_2\text{CO}_3$  ( $\sim 289.6 \text{ eV}$ ) and  $-\text{CO}_2$  ( $\sim 288.5 \text{ eV}$ ) were newly detected, formed from the undesirable reactions between the lithia-based cathode and the electrolyte (such as the decomposition of carbonate solvent in the electrolyte during cycling). The peak intensities of  $\text{Li}_2\text{CO}_3$  and  $-\text{CO}_2$  were reduced by the addition of TMSB, as shown in Fig. 5e. This meant that the surface layer derived from TMSB could suppress undesirable interfacial reactions, which led to the low impedance value of the cells prepared using TMSB added electrolyte, as shown in Fig. 4a. The F 1s spectra of the electrode after one cycle also showed new peaks related to  $\text{Li}_x\text{PO}_y\text{F}_z$  ( $\sim 686.9 \text{ eV}$ ), as shown in Fig. 5d,f, which were associated with the decomposition of the  $\text{LiPF}_6$  salt. The intensity ratio of the LiF/C–F<sub>2</sub> peaks also increased after 1 cycle, which was attributed to the formation of LiF due to the reaction between the cathode (containing superoxides) and the  $\text{LiPF}_6$  salt or the PVDF binder. However, when TMSB added electrolyte was used, the intensity ratio of the LiF/C–F<sub>2</sub> peaks was reduced ( $I_{\text{LiF}}/I_{\text{C-F}_2} = 1.56$ ) compared to that without the TMSB ( $I_{\text{LiF}}/I_{\text{C-F}_2} = 2.35$ ), suggesting that the formation of LiF was suppressed by the TMSB. This may be associated with the protection effect of the interfacial layer derived from the decomposition of TMSB.

Figure 6 shows the C 1s and F 1s spectra of the electrode after 50 cycles. The C 1s spectra near the  $\text{Li}_2\text{CO}_3$  and  $-\text{CO}_2$  peaks were enlarged, as shown in Fig. S4, to compare them after 1 and 50 cycles. Regardless of the type of electrolyte, the intensities of the peaks related to  $\text{Li}_2\text{CO}_3$  and  $-\text{CO}_2$  seemed to increase a little over 50 cycles compared to those during the first cycle. However, it was not significant, as shown in Figs. 6a,c, and S4a–d. This meant that the decomposition of the carbonate solvent and side reactions for the formation of  $\text{Li}_2\text{CO}_3$  did not proceed violently during subsequent cycling, after these reactions occurred during the first cycle. Instead, the intensity of the  $\text{Li}_x\text{PO}_y\text{F}_z$  peaks clearly increased (Fig. 6b,d) during the 50 cycles, indicating that a side reaction

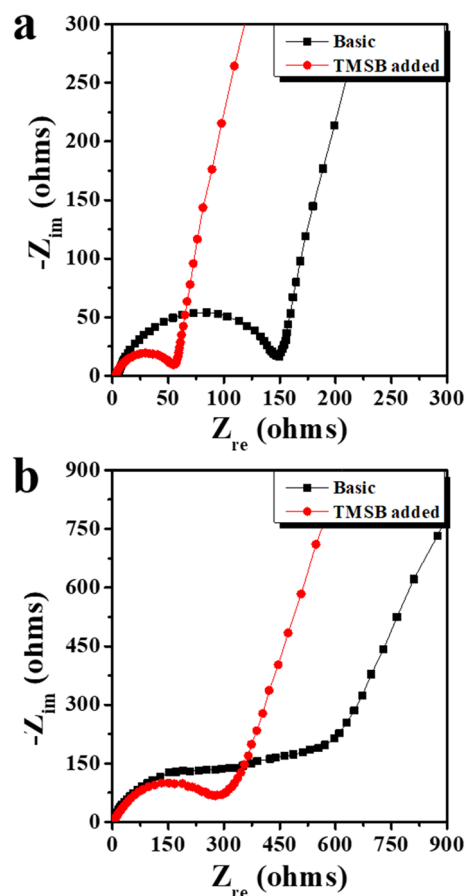


**Figure 4.** Nyquist plots of the cells containing lithia/ $\text{Li}_2\text{RuO}_3$  nanocomposite cycled with a limited capacity of  $600 \text{ mAh}\cdot\text{g}^{-1}$  (a) after 1 cycle, and (b) after 50 cycles.

related to the  $\text{LiPF}_6$  salt actively progressed during cycling. Figure S5 compares the F 1s spectra near the  $\text{Li}_x\text{PO}_y\text{F}_z$  peak after 1 and 50 cycles. A substantial portion of the reaction products formed on the surface of the cathode during cycling could be attributed to the decomposition of the carbonate solvent [such as ethylene carbonate (EC)]. However, in our case, undesirable reactions related to the solvent were not activated during cycling after the formation of the interfacial layer containing  $\text{Li}_2\text{CO}_3$  and  $-\text{CO}_2$  during the initial cycle. This may have been due to the low charging voltage (below 4.0 V) of the lithia-based cathodes.

To further analyse the reaction related to the  $\text{LiPF}_6$  salt, the P 2p spectra of the electrode after 1 and 50 cycles were observed. As shown in Fig. 7a,c, the electrode after one cycle did not show clear peaks in the P 2p spectra. By contrast, as shown in Fig. 7b,d, the spectra of the electrode after 50 cycles exhibited large peaks comprising  $\text{Li}_x\text{POF}_y$  ( $\sim 135.5 \text{ eV}$ ),  $\text{Li}_x\text{PF}_y$  ( $\sim 138.89 \text{ eV}$ ), and phosphate (P-O) ( $\sim 133.7$  and  $134.5 \text{ eV}$ ), which were generated from the decomposition of  $\text{LiPF}_6$ <sup>35</sup>. This showed that the  $\text{LiPF}_6$  salt was continuously decomposed during cycling, which was due to superoxides in the charged lithia-based cathodes being more reactive with the  $\text{LiPF}_6$  salt than with the carbonate solvent during cycling.

It is instructive that the intensity of the  $\text{Li}_x\text{POF}_y$  ( $\sim 135.5 \text{ eV}$ ) and  $\text{Li}_x\text{PF}_y$  ( $\sim 137.8 \text{ eV}$ ) peaks were largely reduced by the addition of TMSB in the electrolyte (Fig. 7d), which indicated that addition of TMSB successfully suppressed the decomposition of the  $\text{LiPF}_6$  salt during cycling. Considering that the side reactions associated with the formation of  $\text{Li}_2\text{CO}_3$  and  $-\text{CO}_2$  were also reduced by the use of TMSB, as shown in Fig. S4, it is clear that the undesirable reactions at the cathode/electrolyte interface were reduced due to the effect of TMSB. It was inferred that the protective layer derived from TMSB effectively reduced the reactivity of the superoxides in the lithia-based cathodes. The superoxides in the charged lithia-based cathode were consumed due to the side reactions with the electrolyte, which led to the capacity fading of the cathode during cycling. However, the addition of TMSB suppressed the loss of superoxides during cycling by reducing undesirable side reactions. As a result, the available capacity, which was obtained without capacity fading during cycling, was increased due to the effect of TMSB.

### Summary

TMSB was introduced as an electrolyte additive to enhance the electrochemical performance of a lithia-based cathode composed of lithia/ $\text{Li}_2\text{RuO}_3$  nanocomposites. Cells prepared using TMSB added electrolyte exhibited increased available capacity as well as improved cyclic performance compared to those using the basic electrolyte. An interfacial layer derived from the TMSB was formed during the initial cycle, which suppressed undesirable

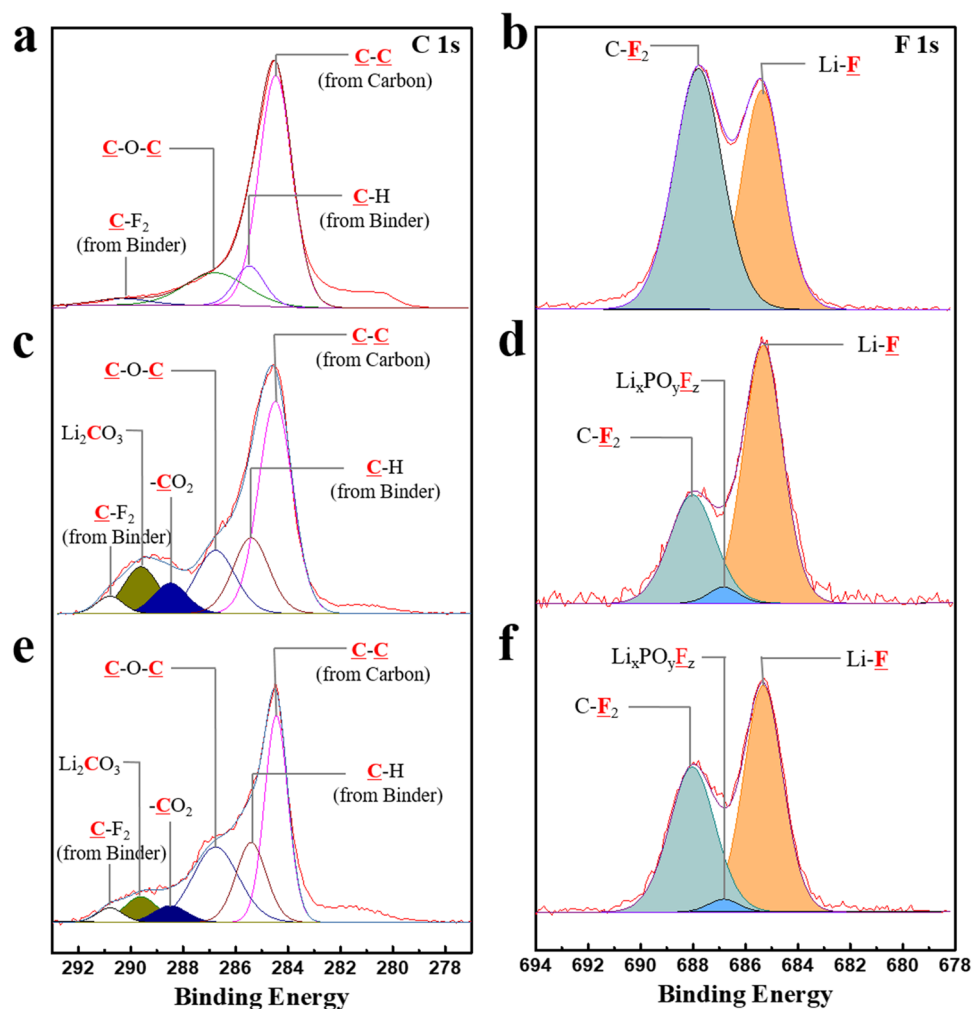


**Figure 5.** XPS profiles of the cathodes composed of lithia/ $\text{Li}_2\text{RuO}_3$  nanocomposite before and after 1 cycle (a) C 1s spectrum of the electrode before the electrochemical test, (b) F 1s spectrum of the electrode before the electrochemical test, (c) C 1s spectrum of the electrode after 1 cycle using the basic electrolyte, (d) F 1s spectrum of the electrode after 1 cycle using the basic electrolyte, (e) C 1s spectrum of the electrode after 1 cycle using TMSB added electrolyte, and (f) F 1s spectrum of the electrode after 1 cycle using TMSB added electrolyte.

side reactions with the electrolyte (such as the decomposition of the  $\text{LiPF}_6$  salt and the formation of  $\text{Li}_2\text{CO}_3$  and  $-\text{CO}_2$ ). We inferred that these side reactions were activated by the superoxides ( $\text{O}^-$  or  $\text{O}^{0.5-}$ ) formed during the charging process in the structure of the lithia-based cathode. Moreover, the suppression of side reactions also reduced the consumption of superoxides during cycling, which resulted in the increased available capacity of the lithia-based cathodes. Figure 8 summarised the effect of the TMSB additives on the electrochemical performance of lithia-based cathodes. This work explains the cause of the increased available capacity due to the use of electrolyte additives, and we trust that it will provide important insights for the active application of electrolyte additives in lithia-based cathodes in the future.

## Methods

To synthesise the  $\text{Li}_2\text{RuO}_3$  used as a catalyst for lithia-based cathodes, pellets composed of a 1:1 (mol%) ratio of  $\text{RuO}_2$  (Alfa Aesar, 99.9%) and  $\text{Li}_2\text{CO}_3$  (Aldrich, 99.99%) were sintered at  $950^\circ\text{C}$  for 24 h. Next, a  $\text{Li}_2\text{RuO}_3$  and lithia mixture comprising Ru content ( $f_{\text{Ru}} = \text{Ru}/(\text{Ru} + \text{Li})$ ) of 0.09 (mol%) was dispersed in butanol to obtain a uniform mixture (Lithia/ $\text{Li}_2\text{RuO}_3$ ) which was then dried under vacuum at  $90^\circ\text{C}$  for 24 h. It was then placed into a sealed zirconia milling container with zirconia balls [5 and 10 mm diameters (1:1 wt%)] in an Ar-glove box and ball-milled using a Planetary Mono Mill (Pulverisette 6, Fritsch) to obtain the lithia/ $\text{Li}_2\text{RuO}_3$  nanocomposites. The milling process was performed for 150 h (resting every 30 min after milling for one hour) at 600 rpm. The lithia/ $\text{Li}_2\text{RuO}_3$  nanocomposite was formed and some of the  $\text{Li}_2\text{RuO}_3$  was decomposed to Ru during this milling process<sup>20</sup>.

For the electrochemical test, the cathode material was mixed with 60 wt% active material (lithia/ $\text{Li}_2\text{RuO}_3$  nanocomposite), 30 wt% Carbon nanotubes, and 10 wt% Polyvinylidene fluoride (PVDF) binder in

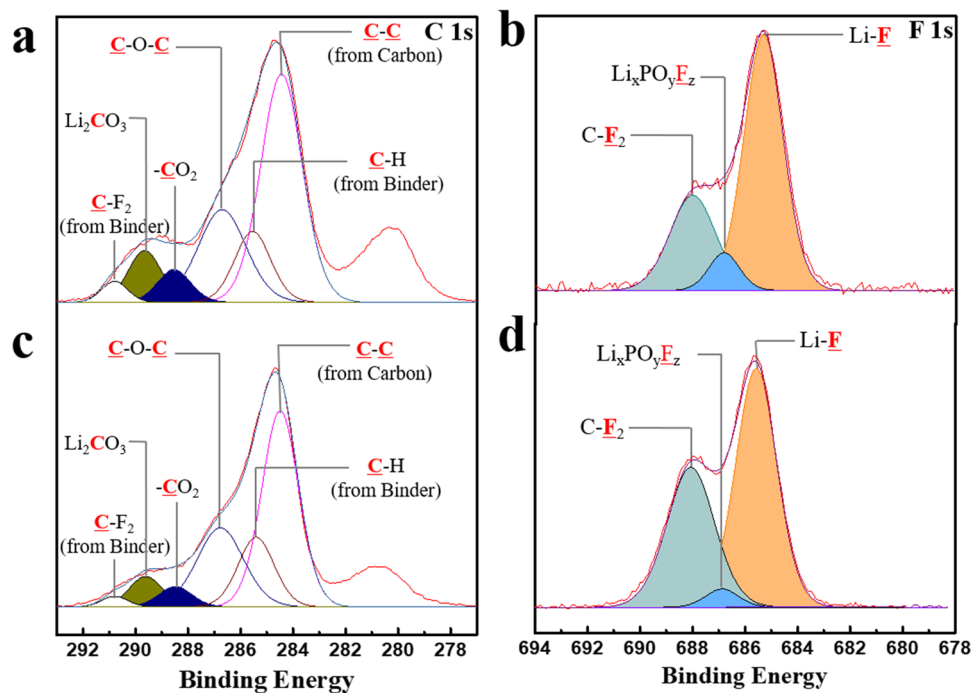


**Figure 6.** XPS profiles of the cathodes composed of lithia/ $\text{Li}_2\text{RuO}_3$  nanocomposite after 50 cycles (a) C 1s spectrum of the electrode after 50 cycles using the basic electrolyte, (b) F 1s spectrum of the electrode after 50 cycles using the basic electrolyte, (c) C 1s spectrum of the electrode after 50 cycles using TMSB added electrolyte, and (d) F 1s spectrum of the electrode after 50 cycles using TMSB added electrolyte.

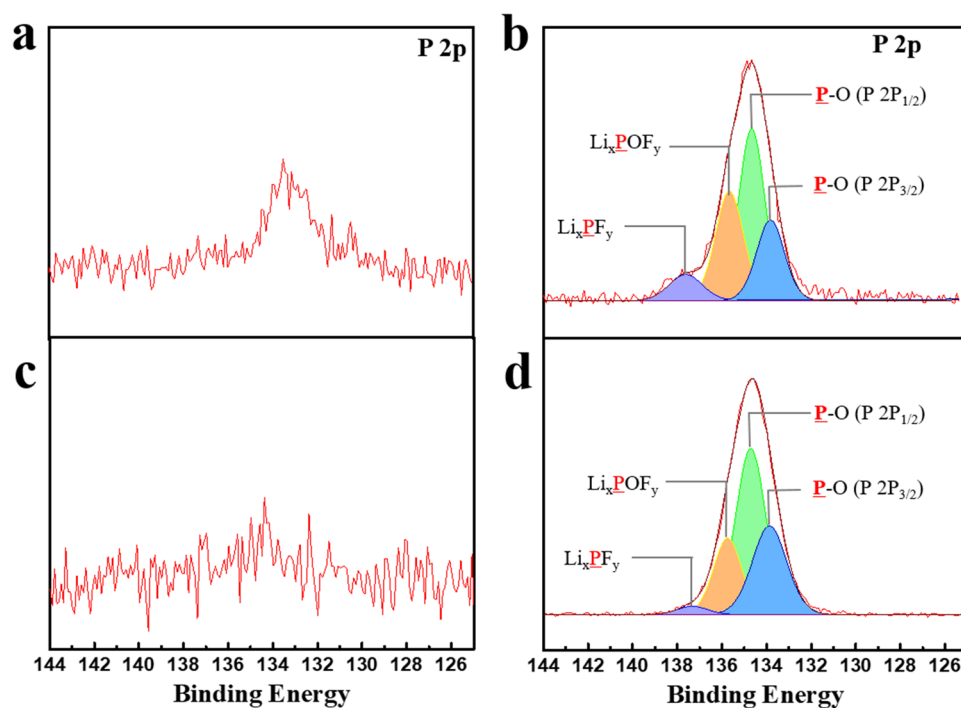


**Figure 7.** Comparison of the XPS profiles of the cathodes composed of lithia/ $\text{Li}_2\text{RuO}_3$  nanocomposite after 1 and 50 cycles (a) P 2p spectrum of the electrode after 1 cycle using the basic electrolyte, (b) P 2p spectrum of the electrode after 50 cycles using the basic electrolyte, (c) P 2p spectrum of the electrode after 1 cycle using TMSB added electrolyte, and (d) P 2p spectrum of the electrode after 50 cycles using TMSB added electrolyte.

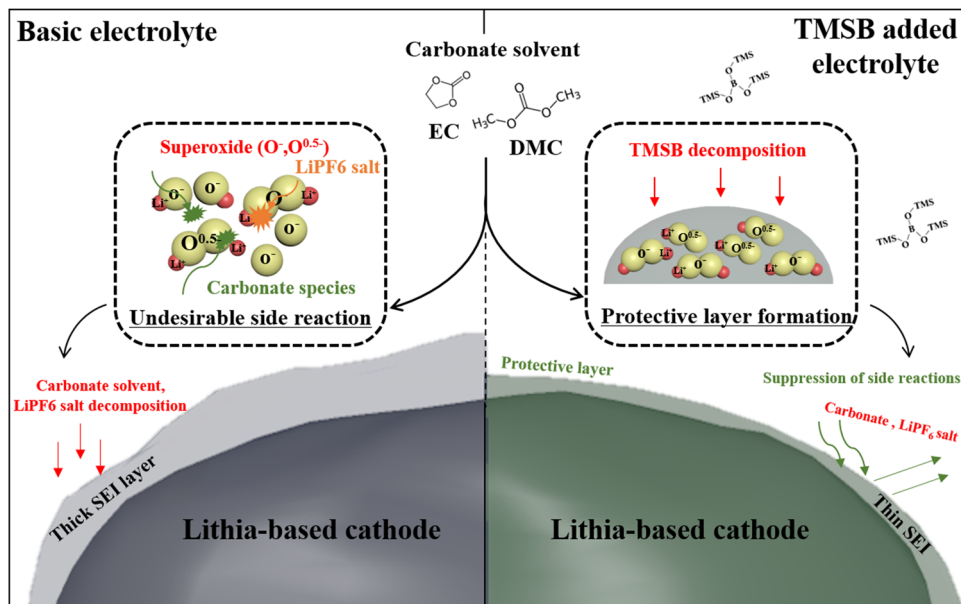


**Figure 8.** Schematic diagram illustrating the effect of TMSB added electrolyte on the electrochemical performance of the lithia-based cathode.

*N*-methyl-2-pyrrolidone (NMP), as the solvent, by ball-milling for 90 min. Next, the mixed slurry was cast on aluminium foil and dried under vacuum at 80 °C for 24 h. The cathode was assembled in a coin cell (2032-type) with Li metal as an anode, an electrolyte, and polypropylene (Celgard 2400) as the separator. For the ‘basic’ electrolyte, 1.0 M LiPF<sub>6</sub> was dissolved in a mixture of EC and dimethyl carbonate (DMC) by volume ratio of 1:1. To obtain tris(trimethylsilyl)borate (TMSB, Aldrich, 99%) added electrolyte, 0.3 wt% of TMSB was dissolved into the electrolyte. The 2032-type coin cells were assembled in an Ar-glove box. The cycle test was conducted with current densities of 50 and 100 mA·g<sup>-1</sup> and a cut-off voltage of 1.8–4.35 V using a WonATech voltammetry system. Impedance measurements were performed using an electrochemical workstation (Ametek, VersaSTAT 3) by applying an AC voltage with an amplitude of 5 mV over a frequency range of 0.1 Hz to 100 kHz. To observe the surface morphology before testing, after the first cycle, and after the 50th cycle, scanning electron microscopy (SEM, JEOL JSM-7610F PLUS) and transmission electron microscopy (TEM, JEOL JEM-2100F, Cs Corrector) were employed. Reaction products on the cathode surface were observed using XPS (Thermo Scientific K-Alpha<sup>+</sup>). XPS was conducted with monochromatised Al K $\alpha$  radiation ( $h\nu = 1,486.6$  eV). A vacuum transfer system was used to avoid moisture/air exposure of the sample during transfer to XPS. The obtained spectra were fitted using XPS peak software (Avantage Data System). The binding energy scale was calibrated using the C 1s peak at 284.6 eV from C–C peak.

Received: 13 May 2020; Accepted: 27 July 2020

Published online: 11 August 2020

## References

- Lee, S. H., Lee, S., Jin, B. S. & Kim, H. S. Optimized electrochemical performance of Ni rich LiNi<sub>0.91</sub>Co<sub>0.06</sub>Mn<sub>0.03</sub>O<sub>2</sub> cathodes for high-energy lithium ion batteries. *Sci. Rep.* **9**, 1–7 (2019).
- Lebens-Higgins, Z. W. *et al.* Surface chemistry dependence on aluminum doping in Ni-rich LiNi<sub>0.8</sub>Co<sub>0.2</sub>- $\gamma$ AlO<sub>2</sub> cathodes. *Sci. Rep.* **9**, 1–12 (2019).
- Park, J. S. & Park, Y. J. Surface modification of a Li[Ni<sub>0.8</sub>Co<sub>0.15</sub>Al<sub>0.05</sub>]O<sub>2</sub> cathode using Li<sub>2</sub>SiO<sub>3</sub> solid electrolyte. *J. Electrochem. Sci. Technol.* **8**, 101–106 (2017).
- Wu, Y. *et al.* Performance and stability improvement of layered NCM lithium-ion batteries at high voltage by a microporous Al<sub>2</sub>O<sub>3</sub> sol-gel coating. *ACS Omega* **4**, 13972–13980 (2019).
- Salitra, G. *et al.* High-performance cells containing lithium metal anodes, LiNi<sub>0.6</sub>Co<sub>0.2</sub>Mn<sub>0.2</sub>O<sub>2</sub> (NCM 622) cathodes, and fluoroethylene carbonate-based electrolyte solution with practical loading. *ACS Appl. Mater. Interfaces* **10**, 19773–19782 (2018).
- Lee, H. *et al.* Characterization and control of irreversible reaction in Li-rich cathode during the initial charge process. *ACS Appl. Mater. Interfaces* **10**, 10804–10818 (2018).
- Sim, S. J., Lee, S. H., Jin, B. S. & Kim, H. S. Improving the electrochemical performances using a V-doped Ni-rich NCM cathode. *Sci. Rep.* **9**, 1–8 (2019).
- McCalla, E. *et al.* Visualization of O–O peroxo-like dimers in high-capacity layered oxides for Li-ion batteries. *Science* (80) **350**, 1516–1521 (2015).
- Yabuuchi, N. *et al.* High-capacity electrode materials for rechargeable lithium batteries: Li<sub>3</sub>NbO<sub>4</sub>-based system with cation-disordered rocksalt structure. *Proc. Natl. Acad. Sci. USA.* **112**, 7650–7655 (2015).
- Freire, M. *et al.* A new active Li–Mn–O compound for high energy density Li-ion batteries. *Nat. Mater.* **15**, 173–177 (2016).
- Okubo, M. & Yamada, A. Molecular orbital principles of oxygen-redox battery electrodes. *ACS Appl. Mater. Interfaces* **9**, 36463–36472 (2017).

12. Luo, K. *et al.* Charge-compensation in 3d-transition-metal-oxide intercalation cathodes through the generation of localized electron holes on oxygen. *Nat. Chem.* **8**, 684–691 (2016).
13. Pearce, P. E. *et al.* Evidence for anionic redox activity in a tridimensional-ordered Li-rich positive electrode  $\beta$ -Li<sub>2</sub>IrO<sub>3</sub>. *Nat. Mater.* **16**, 580–586 (2017).
14. Zhu, Z. *et al.* Anion-redox nanolithia cathodes for Li-ion batteries. *Nat. Energy* **1**, 1–7 (2016).
15. Harada, K. *et al.* Electrochemical reactions and cathode properties of Fe-doped Li<sub>2</sub>O for the hermetically sealed lithium peroxide battery. *J. Power Sour.* **322**, 49–56 (2016).
16. Okuoka, S. I. *et al.* A new sealed lithium-peroxide battery with a co-doped Li<sub>2</sub>O cathode in a superconcentrated lithium bis(fluorosulfonyl)amide electrolyte. *Sci. Rep.* **4**, 1–6 (2014).
17. Kobayashi, H. *et al.* Improved performance of Co-doped Li<sub>2</sub>O cathodes for lithium-peroxide batteries using LiCoO<sub>2</sub> as a dopant source. *J. Power Sour.* **306**, 567–572 (2016).
18. Kobayashi, H. *et al.* Synthesis of Cu-doped Li<sub>2</sub>O and its cathode properties for lithium-ion batteries based on oxide/peroxide redox reactions. *J. Power Sour.* **340**, 365–372 (2017).
19. Lee, S. Y. & Park, Y. J. Lithia/(Ir, Li<sub>2</sub>IrO<sub>3</sub>) nanocomposites for new cathode materials based on pure anionic redox reaction. *Sci. Rep.* **9**, 1–10 (2019).
20. Lee, B. G. & Park, Y. J. Lithia-based nanocomposites activated by Li<sub>2</sub>RuO<sub>3</sub> for new cathode materials rooted in the oxygen redox reaction. *Nanoscale Res. Lett.* **14**, 1–10 (2019).
21. Ohta, N. *et al.* Enhancement of the high-rate capability of solid-state lithium batteries by nanoscale interfacial modification. *Adv. Mater.* **18**, 2226–2229 (2006).
22. Lee, J. W. & Park, Y. J. Surface modification of Li[Ni<sub>0.8</sub>Co<sub>0.15</sub>Al<sub>0.05</sub>]O<sub>2</sub> cathode using a Li<sub>2</sub>ZrO<sub>3</sub>/polydopamine double layer. *Sci. Adv. Mater.* **10**, 835–844 (2018).
23. Zuo, D., Tian, G., Li, X., Chen, D. & Shu, K. Recent progress in surface coating of cathode materials for lithium ion secondary batteries. *J. Alloy. Compd.* **706**, 24–40 (2017).
24. Kwak, H. W. & Park, Y. J. Li<sub>2</sub>MoO<sub>4</sub> coated Ni-rich cathode for all-solid-state batteries. *Thin Solid Films* **660**, 625–630 (2018).
25. Zhang, J., Li, Z., Gao, R., Hu, Z. & Liu, X. High rate capability and excellent thermal stability of Li<sup>+</sup>-conductive Li<sub>2</sub>ZrO<sub>3</sub>-coated LiNi<sub>1/3</sub>Co<sub>1/3</sub>Mn<sub>1/3</sub>O<sub>2</sub> via a synchronous lithiation strategy. *J. Phys. Chem. C* **119**, 20350–20356 (2015).
26. Kwak, H. W. & Park, Y. J. Cathode coating using LiInO<sub>2</sub>-LiI composite for stable sulfide-based all-solid-state batteries. *Sci. Rep.* **9**, 1–9 (2019).
27. Kim, H., Byun, D., Chang, W., Jung, H. G. & Choi, W. A nano-LiNbO<sub>3</sub> coating layer and diffusion-induced surface control towards high-performance 5 v spinel cathodes for rechargeable batteries. *J. Mater. Chem. A* **5**, 25077–25089 (2017).
28. Lee, S. Y. & Park, Y. J. Effect of vinylene carbonate and fluoroethylene carbonate electrolyte additives on the performance of lithia-based cathodes. *ACS Omega* **5**, 3579–3587 (2020).
29. Kobayashi, H. *et al.* Cathode performance of co-doped Li<sub>2</sub>O with specific capacity (400 mAh/g) enhanced by vinylene carbonate. *J. Electrochem. Soc.* **164**, A750–A753 (2017).
30. Zuo, X. *et al.* Effect of tris(trimethylsilyl)borate on the high voltage capacity retention of LiNi<sub>0.5</sub>Co<sub>0.2</sub>Mn<sub>0.3</sub>O<sub>2</sub>/graphite cells. *J. Power Sour.* **229**, 308–312 (2013).
31. Rong, H. *et al.* Tris(trimethylsilyl) borate (TMSB) as a cathode surface film forming additive for 5v Li/LiNi<sub>0.5</sub>Mn<sub>1.5</sub>O<sub>4</sub> Li-ion cells. *Electrochim. Acta* **147**, 31–39 (2014).
32. Li, J. *et al.* Tris(trimethylsilyl)borate as an electrolyte additive for improving interfacial stability of high voltage layered lithium-rich oxide cathode/carbonate-based electrolyte. *J. Power Sour.* **285**, 360–366 (2015).
33. Liu, Y., Tan, L. & Li, L. Tris(trimethylsilyl) borate as an electrolyte additive to improve the cyclability of LiMn<sub>2</sub>O<sub>4</sub> cathode for lithium-ion battery. *J. Power Sour.* **221**, 90–96 (2013).
34. Wang, Y. *et al.* Improving cycling performance of LiCoPO<sub>4</sub> cathode material by adding tris(trimethylsilyl) borate as electrolyte additive. *J. Electroanal. Chem.* **802**, 8–14 (2017).
35. Cha, J., Han, J. G., Hwang, J., Cho, J. & Choi, N. S. Mechanisms for electrochemical performance enhancement by the salt-type electrolyte additive, lithium difluoro(oxalato)borate, in high-voltage lithium-ion batteries. *J. Power Sour.* **357**, 97–106 (2017).
36. Wang, L. *et al.* 1,3,6-Hexanetricarbonitrile as electrolyte additive for enhancing electrochemical performance of high voltage Li-rich layered oxide cathode. *J. Power Sour.* **361**, 227–236 (2017).
37. Kim, K. *et al.* Dual-function ethyl 4,4,4-trifluorobutyrate additive for high-performance Ni-rich cathodes and stable graphite anodes. *J. Power Sour.* **396**, 276–287 (2018).
38. Edström, K., Gustafsson, T. & Thomas, J. O. The cathode-electrolyte interface in the Li-ion battery. in *Electrochimica Acta* Vol. 50 397–403 (Pergamon, 2004).

## Acknowledgements

This work was supported by the National Research Foundation of Korea(NRF) grant funded by the Korea government (MSIT) (No. 2020R1A2C1008370) and supported by the Technology Innovation Program (20007034) funded by the Ministry of Trade, Industry & Energy (MOTIE, Korea).

## Author contributions

Y.J.P. designed the overall research. B.G.L. conducted the experiments. B.G.L. and Y.J.P. wrote the manuscript together.

## Competing interests

The authors declare no competing interests.

## Additional information

**Supplementary information** is available for this paper at <https://doi.org/10.1038/s41598-020-70333-2>.

**Correspondence** and requests for materials should be addressed to Y.J.P.

**Reprints and permissions information** is available at [www.nature.com/reprints](http://www.nature.com/reprints).

**Publisher's note** Springer Nature remains neutral with regard to jurisdictional claims in published maps and institutional affiliations.



**Open Access** This article is licensed under a Creative Commons Attribution 4.0 International License, which permits use, sharing, adaptation, distribution and reproduction in any medium or format, as long as you give appropriate credit to the original author(s) and the source, provide a link to the Creative Commons license, and indicate if changes were made. The images or other third party material in this article are included in the article's Creative Commons license, unless indicated otherwise in a credit line to the material. If material is not included in the article's Creative Commons license and your intended use is not permitted by statutory regulation or exceeds the permitted use, you will need to obtain permission directly from the copyright holder. To view a copy of this license, visit <http://creativecommons.org/licenses/by/4.0/>.

© The Author(s) 2020